.

Technical Report ♯2003 – 3

MODELING AND SIMULATION OF IEEE 14 BUS SYSTEM WITH FACTS CONTROLLERS

Sameh Kamel Mena Kodsi, IEEE Student Member

Claudio A. Cañizares, IEEE Senior Member

ABSTRACT

This report covers the modeling of the standard IEEE 14 bus system using the Power System Toolbox (PST) package. The basic system is tested under large and small disturbances to study the dynamic behavior of the system and the stability margins associated with the different configurations of the system.

As a suggested solution to increase stability margins of the system, FACTS controllers are added, modeled and tested to show the effect of these controllers on the different stability margins under both large and small disturbances.

Contents

List of Figures

List of Tables

Chapter 1

BLOCK DIAGRAM MODELING

1.1 Introduction

A single line diagram of the IEEE 14-bus standard system extracted from [1] is shown in Figure 1.1. It consists of five synchronous machines with IEEE type-1 exciters, three of which are synchronous compensators used only for reactive power support. There are 11 loads in the system totaling 259 MW and 81.3 Mvar. The dynamic data for the generators exciters was selected from [2].

The IEEE 14-BUS was studied using the UWPFLOW and PST programs to obtain the system P-V curves and perform time domain and eigenvalue analyses to study the general performance of the system. SVC, TCSC and PSS controllers were also added to the system, as shown in Figure 1.2, to study their effect in the system and their interactions. The model details are discussed in the following sections, and the corresponding data is given in Appendices A and B.

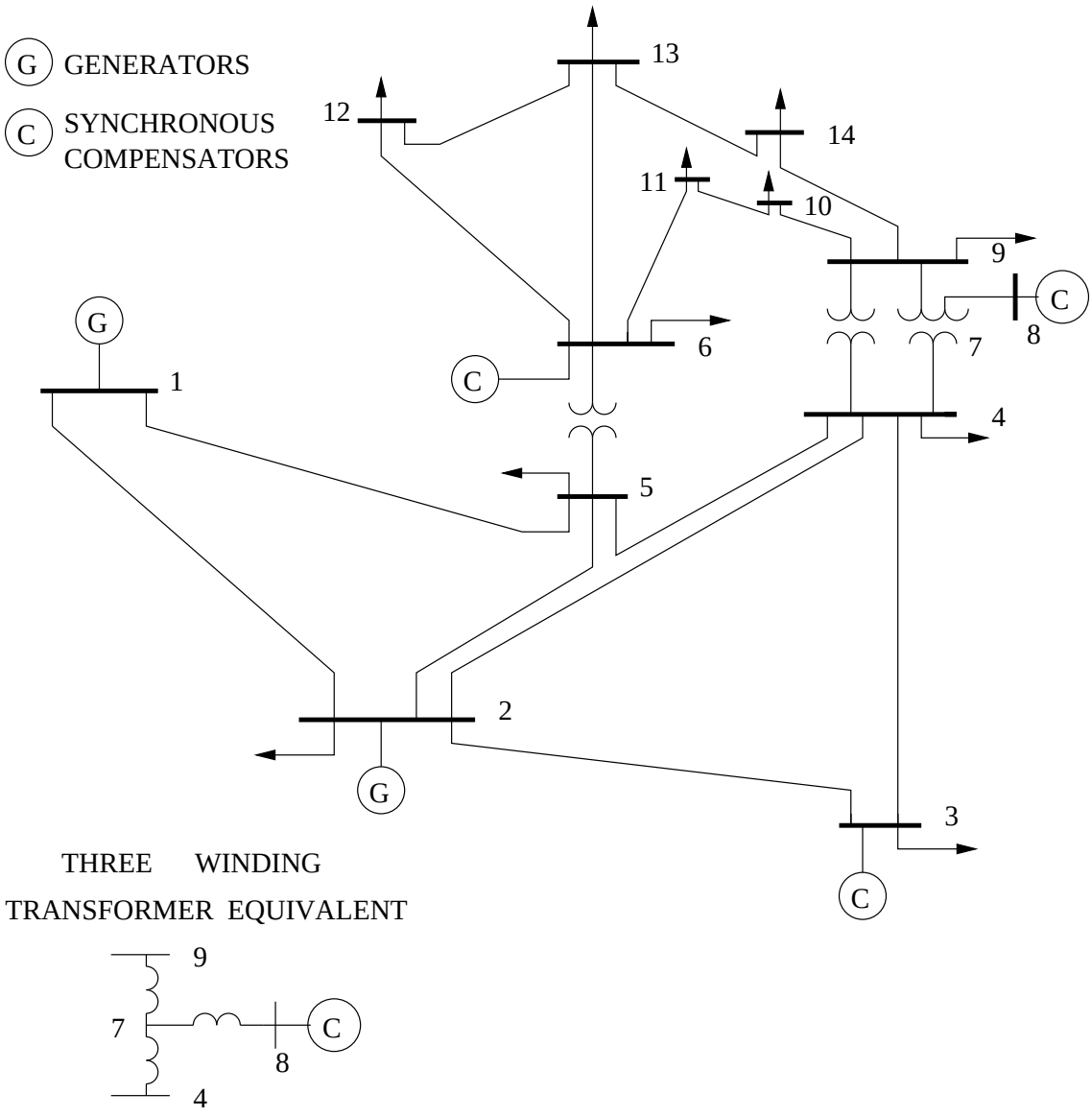

Figure 1.1: IEEE 14-bus test system.

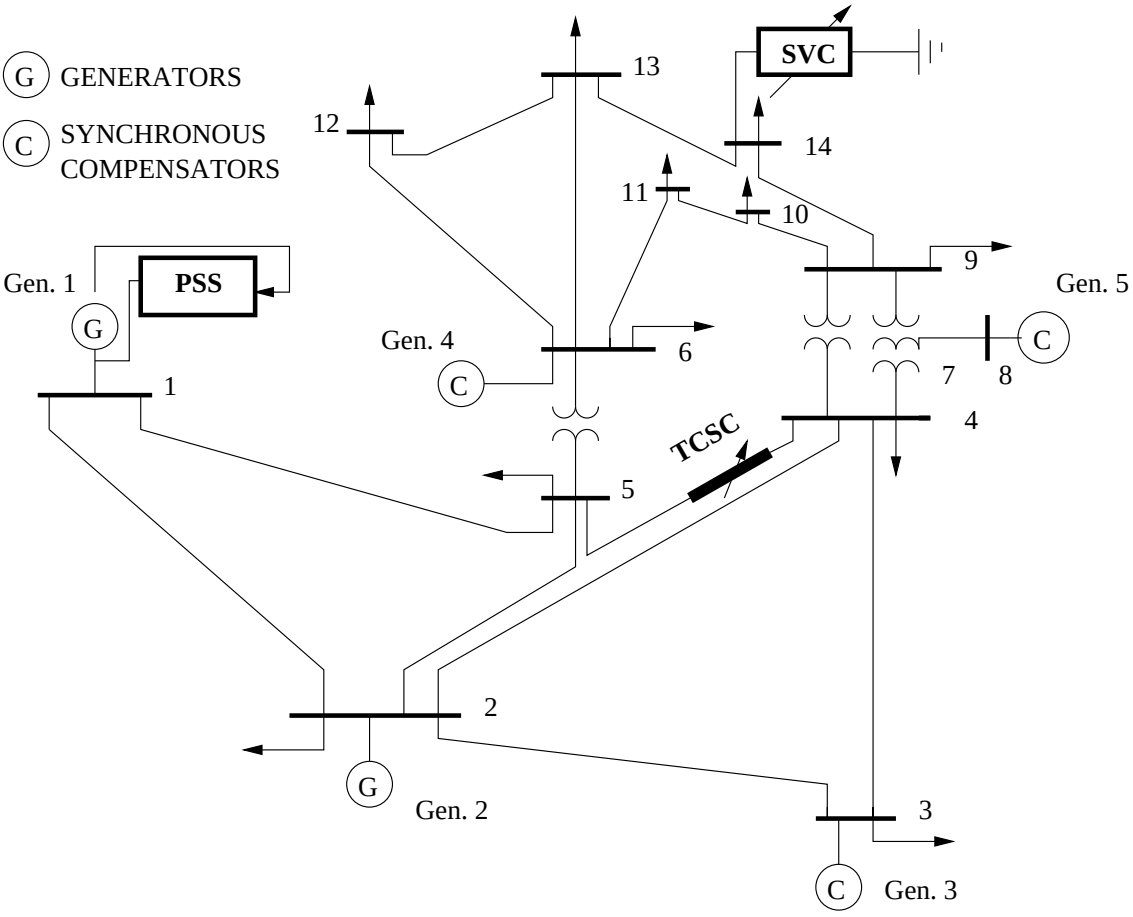

Figure 1.2: IEEE 14-bus test system with different controllers.

The detailed data of the system is shown in Appendix A.

1.2 System Models

1.2.1 Synchronous Generators Model

Mathematical models of a synchronous machine vary from elementary classical models to more detailed ones. In the detailed models, transient and subtransient

phenomena are considered [3, 4]. In the PST program, the subtransient detailed models are used to represent the machines in the system as depicted in Figure 1.3 [5].

This model is rearranged as shown in Figure 1.4 [6], illustrating the relation between the equivalent circuit subtransient variables. The following equations link the mechanical variables with the electrical variables, and result in the block diagram representation depicted in Figure 1.5:

$$\begin{aligned} (D \ + \ \tau_j S) \ &= T_m \ - \ (E''_q \ I_q + E''_d \ I_d) \\ S\delta \ &= \omega \ - \ 1 \end{aligned} \tag{1.1}$$

where D and τ_j represent the damping constant and the inertia time constant, respectively; T_m stands for the input mechanical torque; ω and δ represent the rotational speed and rotor angle, respectively; E''_d and E''_q correspond to the subtransient generated voltage in the direct and quadrature axes, and I_d and I_q stand for the armature current in the direct and quadrature axes.

For eigenvalue or time domain simulation studies, it is necessary to include the effects of the excitation controller, which indirectly controls the reactive output of a generator. A simple Automatic Voltage Regulator (AVR) model is used in PST to represent the excitation control of generators, as shown in Figure 1.6 [6].

1.2.2 Load Models

The modeling of loads in stability studies is a complex problem due to the unclear nature of aggregated loads (e.g. a mix of fluorescent, compact fluorescent, incandescent lamps, refrigerators, heater, motor, etc.). Load models are typically classified into two broad categories: static and dynamic. The loads can be modeled using

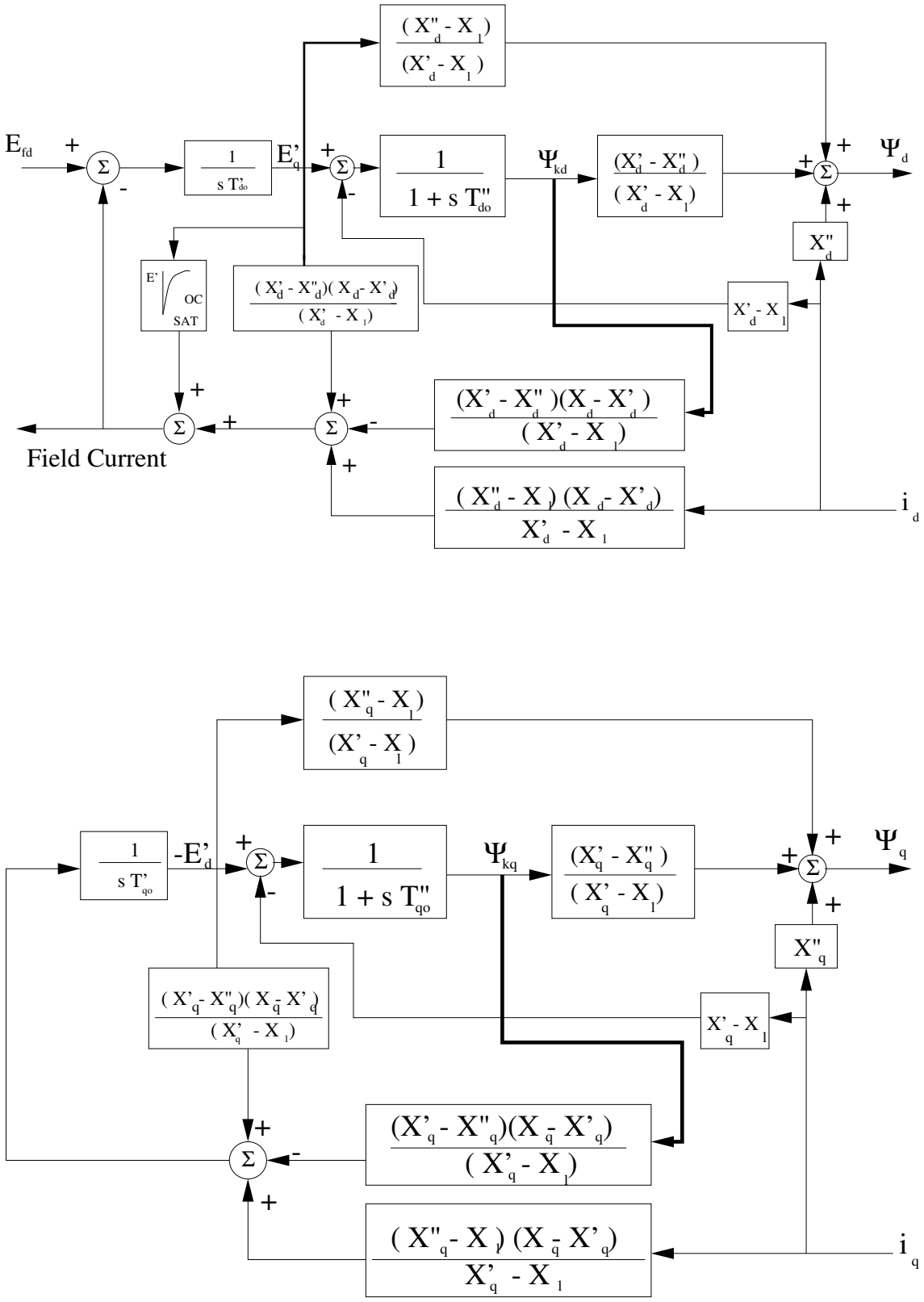

Figure 1.3: Subtransient model for the synchronous generator in the direct and quadrature.

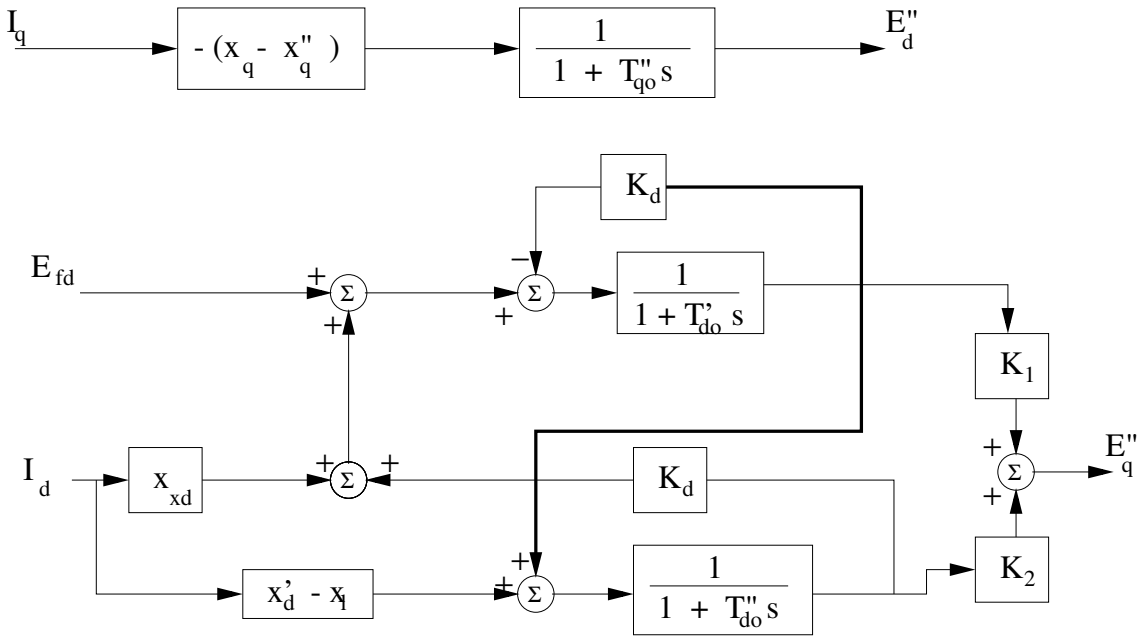

Figure 1.4: Rearranged block diagram for the subtransient machine model.

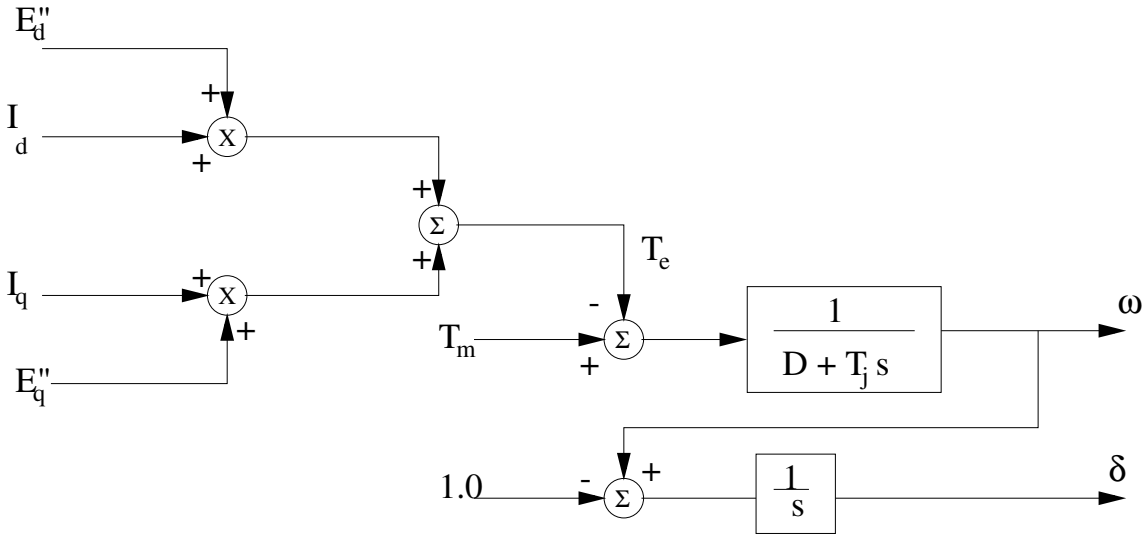

Figure 1.5: Block diagram for computation of torque and speed in the subtransient machine model.

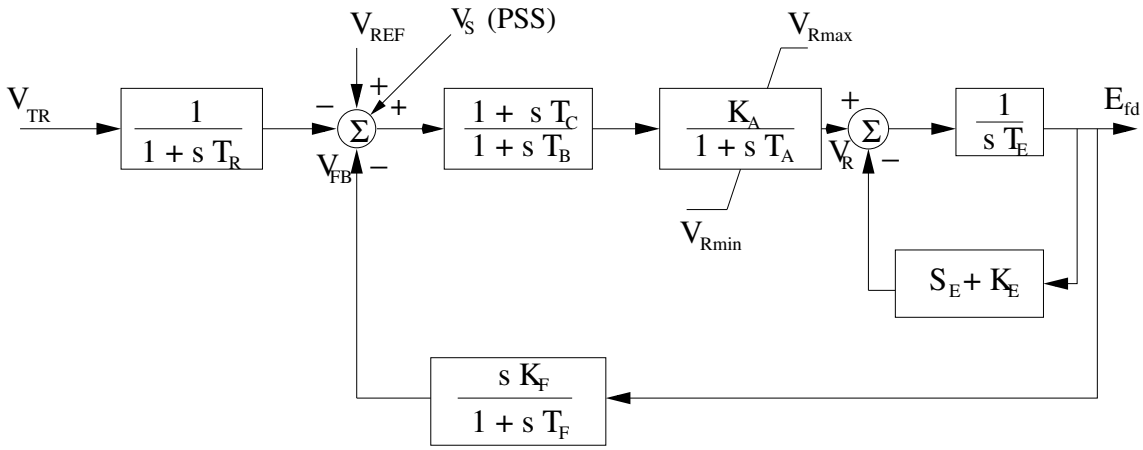

Figure 1.6: AVR and exciter model for synchronous generator.

constant impedance, constant current and constant power static load models [7]. Thus,

1. *Constant Impedance Load Model (constant Z)*: A static load model where the real and reactive power is proportional to the square of the voltage magnitude. It is also referred to constant admittance load model.

2. *Constant Current Load Model (constant I)*: A static load model where the real and reactive power is directly proportional to the voltage magnitude.

3. *Constant Power Load Model (constant PQ)*: A static load model where the real and reactive powers have no relation to the voltage magnitude. It is also referred a constant MVA load model.

All these load models can be described by the following polynomial equations:

$$\begin{aligned} P =& P_0 \left(\frac{V}{V_0}\right)^a \\ Q =& Q_0 \left(\frac{V}{V_0}\right)^b \end{aligned} \tag{1.2}$$

where P_0 and Q_0 stand for the real and reactive powers consumed at a reference voltage V_0. The exponents a and b depend on the type of load that is being represented, e.g. for constant power load models $a = b = 0$, for constant current load models $a = b = 1$ and for constant impedance load models $a = b = 2$.

In power flow studies and to obtain the corresponding P-V curves, the loads are typically represented as constant PQ loads with constant power factor, and increased according to:

$$\begin{aligned} P_L &= P_{Lo}(1 + \lambda) \\ Q_L &= Q_{Lo}(1 + \lambda) \end{aligned} \tag{1.3}$$

where P_{Lo} and Q_{Lo} are the initial real and reactive power respectively and λ is a p.u. loading factor, which represents a slow varying parameter typically used in voltage stability studies.

1.2.3 Power System Stabilizer PSS Model

A PSS can be viewed as an additional control block used to enhance the system stability [6]. This block is added to the AVR, and uses stabilizing feedback signals such as shaft speed, terminal frequency and/or power to change the input signal of the AVR.

The three basic blocks of a typical PSS model, are illustrated in Figure 1.7. The first block is the stabilizer Gain block, which determines the amount of damping. The second is the Washout block, which serves as a high-pass filter, with a time constant that allows the signal associated with oscillations in rotor speed to pass unchanged, but does not allow the steady state changes to modify the terminal voltages. The last one is the phase-compensation block, which provides the desired

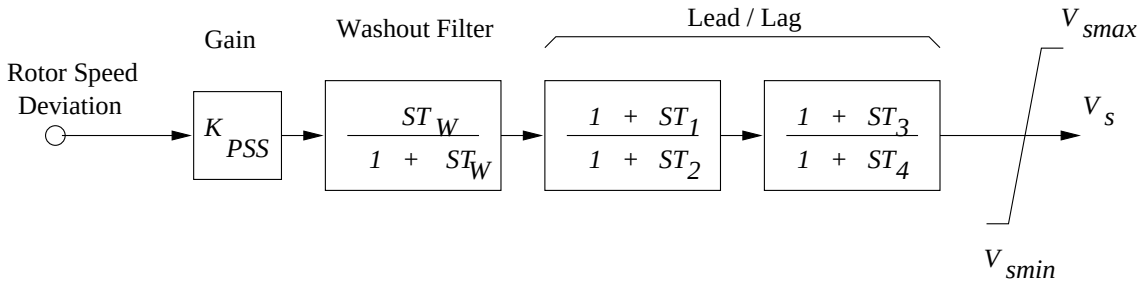

Figure 1.7: Basic block PSS diagram.

phase-lead characteristic to compensate for the phase lag between the AVR input and the generator electrical (air-gap) torque; in practice, two or more first-order blocks may be used to achieve the desired phase compensation.

1.2.4 FACTS Controllers Models

FACTS controllers are a family of electronic controllers used to enhance power system performance [8]. Certain FACTS controllers have already been applied and others are under development. In particular, SVC, TCSC, STATCOM, SSSC and UPFC (a combination of a SSSC and a STATCOM) are the best known FACTS controllers [9, 10, 11, 12, 13, 14, 15]. A brief description regarding the SVC and TCSC models used follows.

SVC

The main job of a SVC is to inject a controlled capacitive or inductive current so as to maintain or control a specific variable, mainly bus voltage [8]. A well-known configuration of a SVC are the Fixed Capacitor (FC) with Thyristor Controlled reactor (TCR), and Thyristor Switched Capacitor (TSC) with TCR. Figures 1.8

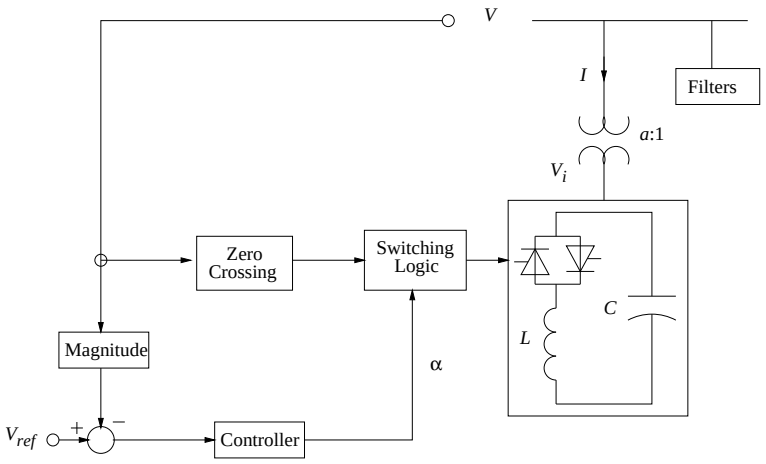

Figure 1.8: Basic SVC structure with voltage control.

and 1.9 show a basic structure of a SVC with voltage control and its steady state control characteristic, respectively, for an FC-TCR type SVC [16].

The SVC is typically modeled using a variable reactance with maximum inductive and capacitive limits (see Figure 1.10), which directly correspond to the limits in the firing angles of the thyristors. In addition to the main job of the SVC controller, which is to control the SVC bus voltage, the reactance of the SVC controller maybe used to damp system oscillations, as denoted in Figure 1.10 by "SVC-sig".

TCSC

A TCSC controller is basically a TCR in parallel with a bank of capacitors. A typical single module TCSC structure for current control is shown in Figure 1.11; the corresponding steady state V-I characteristic is shown in Figure 1.12 [16, 17].

In a TCSC, two main operational blocks can be clearly identified, i.e. an external control and an internal control [17]. The function of the external control is to operate the controller to fullfill specified compensation objectives; this control

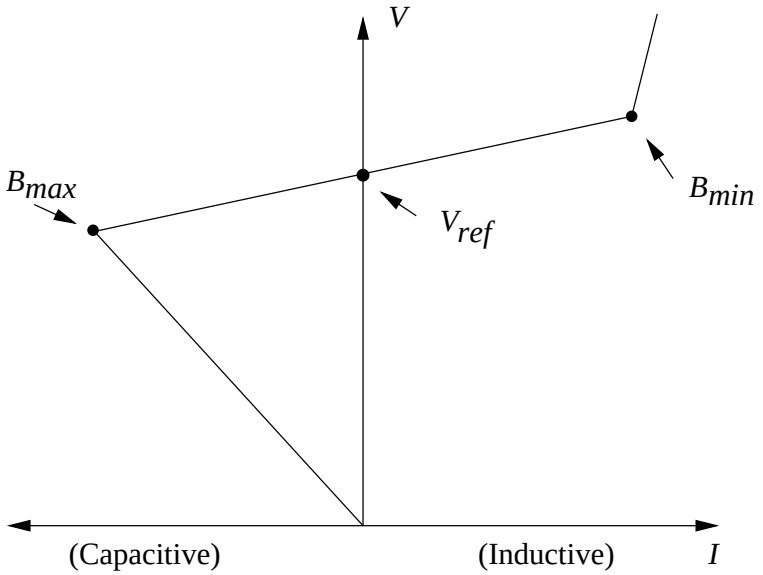

Figure 1.9: Typical steady-state voltage control characteristic of an SVC.

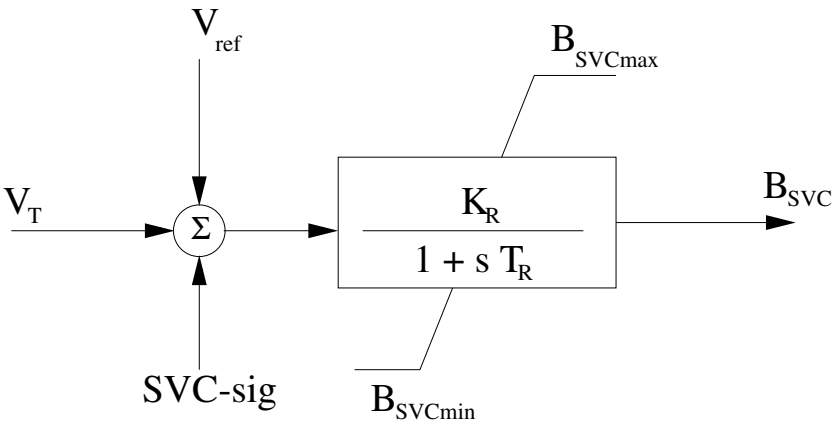

Figure 1.10: Block diagram of an SVC used in PST.

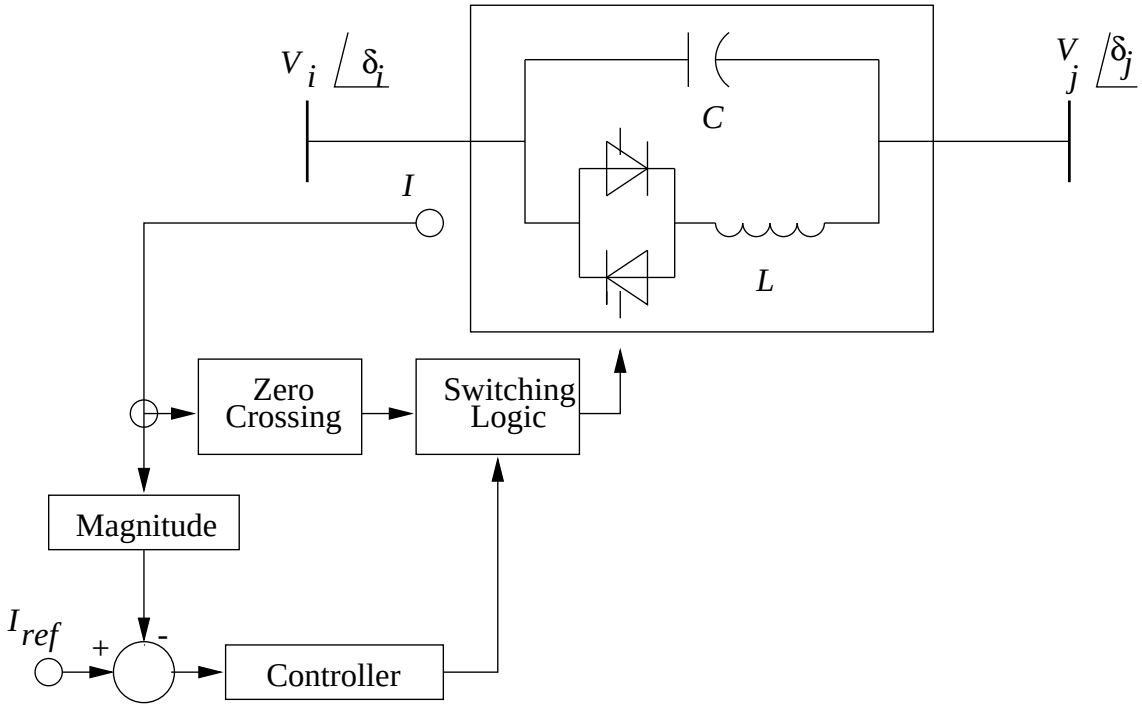

Figure 1.11: Basic TCSC structure with current control.

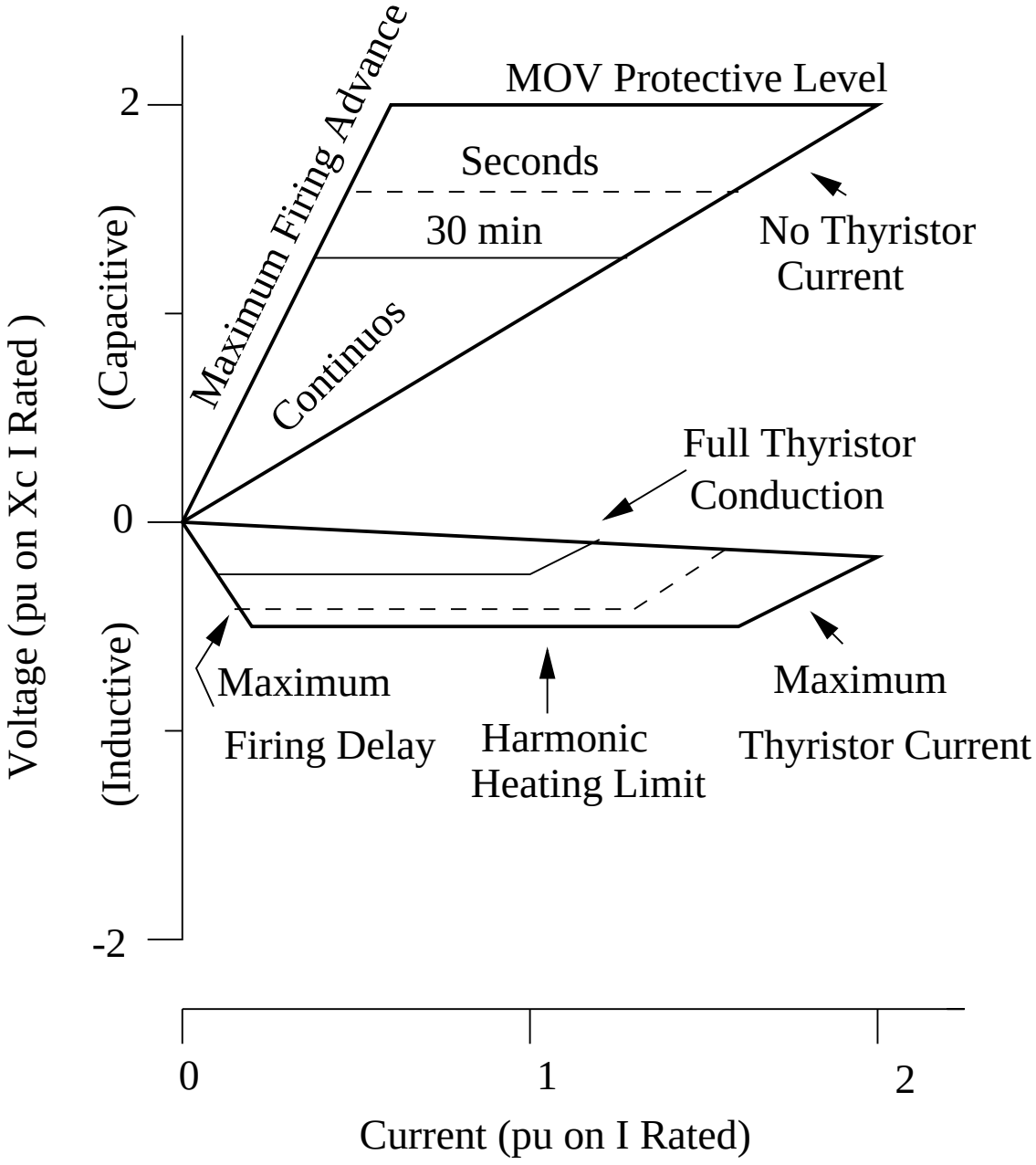

Figure 1.12: TCSC V-I steady state characteristics.

directly depends on measured systems variables to define the reference for the internal control, which is defined by the value of the controller reactance. The function of the internal control is to provide the right gate drive signals for the thyristor valve to produce the appropriate compensating reactance. Thus, the functional operation of the controller is defined by the external control [17, 18].

The external control is defined by the control objectives. The typical steady state function of a TCSC is reactance control, but additional functions for stability improvement, such as damping controls, may be included in this control. Another steady state control that has been discussed in the literature is power flow control, which is usually achieved either automatically with a "slow" PI controller or manually through direct operator supervision [19].

The general block diagram of the TCSC model and external control structure used here is shown in Figure 1.13 [20]. In this figure, X_m is defined by the stability control modulation reactance value which is determined by the stability or dynamic control loop, and X_{eo} stands for the TCSC steady state reactance or set point, whose value is provided by the steady state control loop. The sum of these two values results in X'_m, which is the net reactance order from the external control block. As the natural response of the device internal control is characterized by the delayed action, this signal is put through a first-order lag that yields the equivalent capacitive reactance X_e of the TCSC [21]. The steady state control loop may have a large time constant or be adjusted manually; hence, for large-disturbance transients, X_{eo} is assumed here to be constant. The equivalent reactance of TCSC is a function of the firing angle α, based on the assumption of a sinusoidal steady-state controller current; hence, the operating limits are defined by the limits of firing angle α. The range of the equivalent reactance is $X_{emin} \leq X_e \leq X_{emax}$, with $X_{emax} = X_e\ (\alpha_{min})$ and $X_{emin} = X_e\ (180^o) = X_c$, where X_c is the reactance of TCSC capacitor.

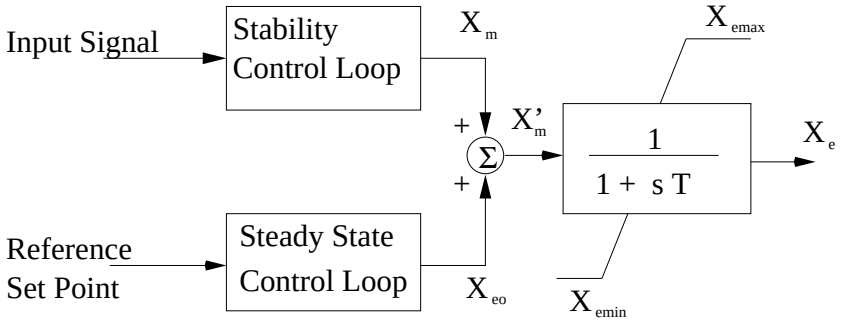

Figure 1.13: TCSC model for stability studies.

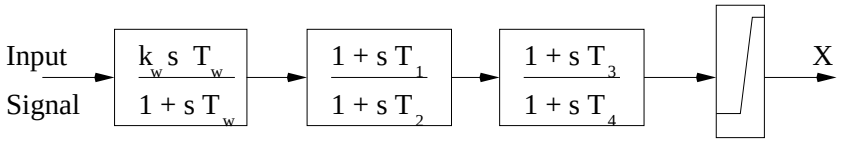

Figure 1.14: Block diagram of the TCSC stability control loop.

The general structure of the stability controller is shown in Figure 1.14 [20]. It consists of a washout filter, a dynamic compensator, and a limiter. The washout filter is used to avoid a controller response to the dc offest of the input signal. The dynamic compensator consists of two (or more) lead-lag blocks to provide the necessary phase-lead characteristics. Finally, the limiter is used to improve controller response to large deviations in the input signal.

Chapter 2

TOOLS AND SIMULATION RESULTS

2.1 Introduction

This report presents a series of results associated with stability issues of the base test system and the inclusion of some controllers. For small perturbation, one can determine the available Static Load Margin (SLM), which is the maximum loading level beyond which steady state solutions cannot be obtained for the system. This is accomplished by obtaining full P-V curves for normal and contingency (e.g. line outages) conditions. On these P-V curves, Dynamic Load Margins (DLM), which are typically the loading levels at which the system presents oscillatory instabilities associated with Hopf bifurcations, are also depicted. A mix of continuation power flow and eigenvalue analysis tools are used to determine these P-V curves and associated SLM and DLM values.

The ability of the system to maintain a stable operation condition under large

perturbations (e.g. line outages) at different loading conditions is typically studied using time domain simulation tools.

2.2 Tools

All P-V curves were obtained using the University of Waterloo Power Flow (UW-PFLOW) package [22]. A variety of output files permit further analyses, such as tangent vectors, left and right eigenvectors at the bifurcation point, power flow solutions at different loading levels, and voltage stability indices.

The eigenvalues and eigenvectors of the test systems were calculated here by means of the Power System Toolbox (PST) [23, 24]. For time domain simulations, the transient stability analysis module of PST was used. The transient stability analysis module of PST uses a predictor-corrector method for solving the differential-algebraic equations resulting from the system models utilized for the simulation presented here. This module also accommodates any user-defined models.

2.3 Simulation Results

2.3.1 Base Test System Performance

For the IEEE 14-bus system, the P-V curves for various cases, with and without different FACTS controllers, were obtained. Table 2.1 illustrates the DLM and SLM associated with P-V curves shown in Figure 2.1, the base case and for line 2-4 and line 2-3 outages. In these curves, Hopf bifurcation (HB) points, which were obtained through eigenvalue analysis, are also depicted. The vertical line shown

Table 2.1: Dynamic and Static Loading Margins for Base Test System

	Base Case	Line 2-4 Outage	Line 2-3 Outage
DLM (p.u.)	0.46	0.35	0.14
SLM (p.u.)	0.71	0.53	0.26

represents the load level in the system, assuming that almost all loads were modeled as constant PQ loads [25], as these are the type of loads that create the most stress in the system (only buses 5 and 14 were modeled as a constant impedance loads due to constraints associated with modeling FACTS controllers in the simulation program PST).

In order to study the behavior of the system under large perturbations, a time domain simulation and eigenvalue computation were performed for a line 2-4 outage at the operating point defined by $\lambda = 0.4$. Thus, Figure 2.2 shows the eigenvalues for the line outage, whereas Figure 2.3 shows the corresponding time domain simulations. From these figures, one can conclude that line 2-4 outage leads the system to an oscillatory unstable condition.

Various power system controllers are used to control the oscillatory problem associated with the Hopf bifurcations [25], namely a PSS and a TCSC. On the other hand a SVC was added to the system to improve voltage stability [12]. The system behavior corresponding to the insertion of each controller is discussed below.

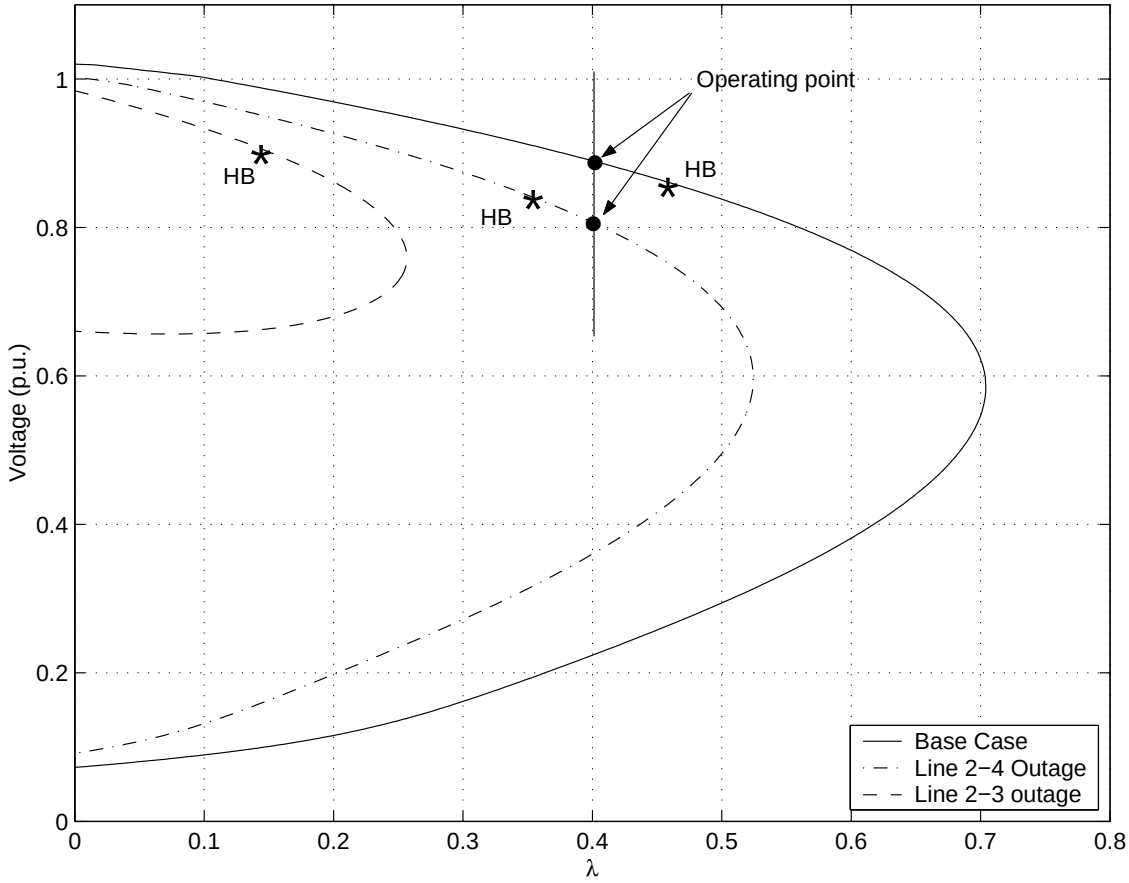

Figure 2.1: P-V curves at bus 14 for different contingencies for the IEEE 14-bus test system.

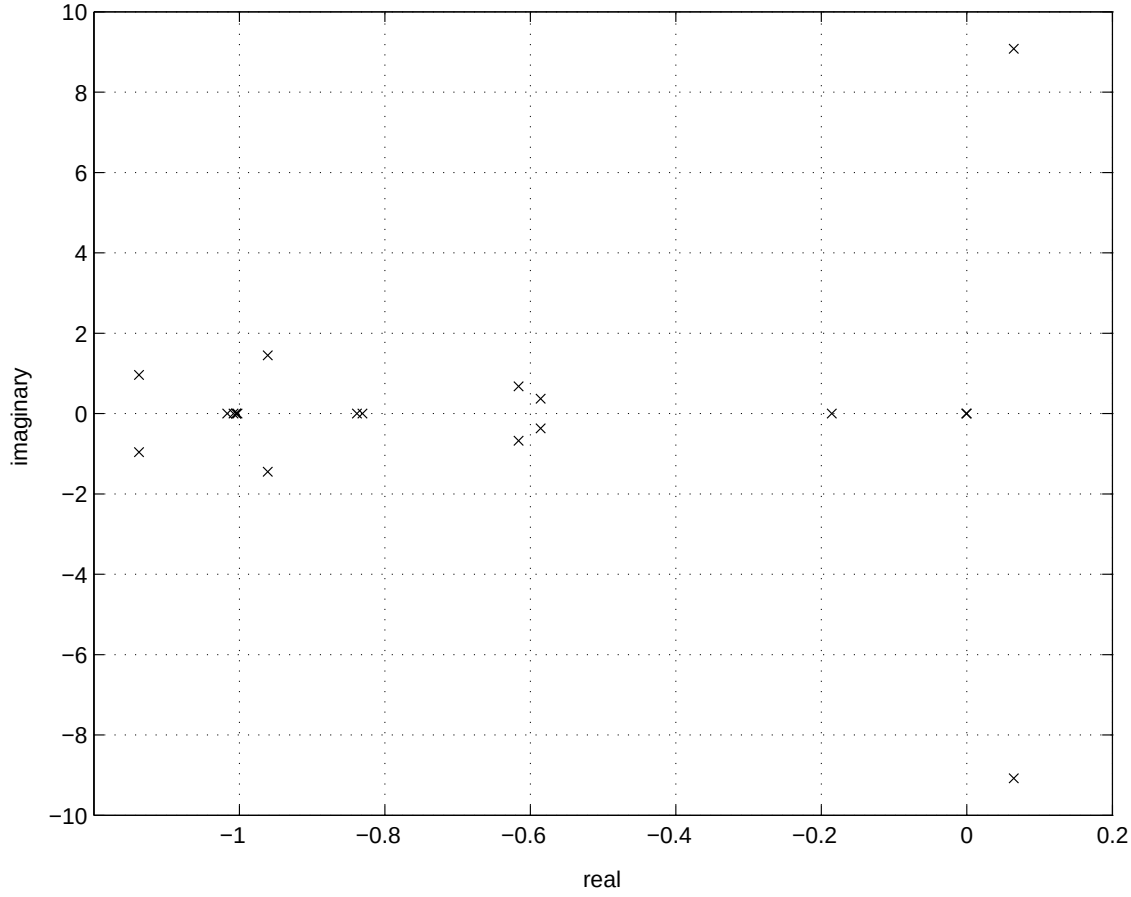

Figure 2.2: Eigenvalues for the line 2-4 outage in the IEEE 14-bus test system at λ=0.4.

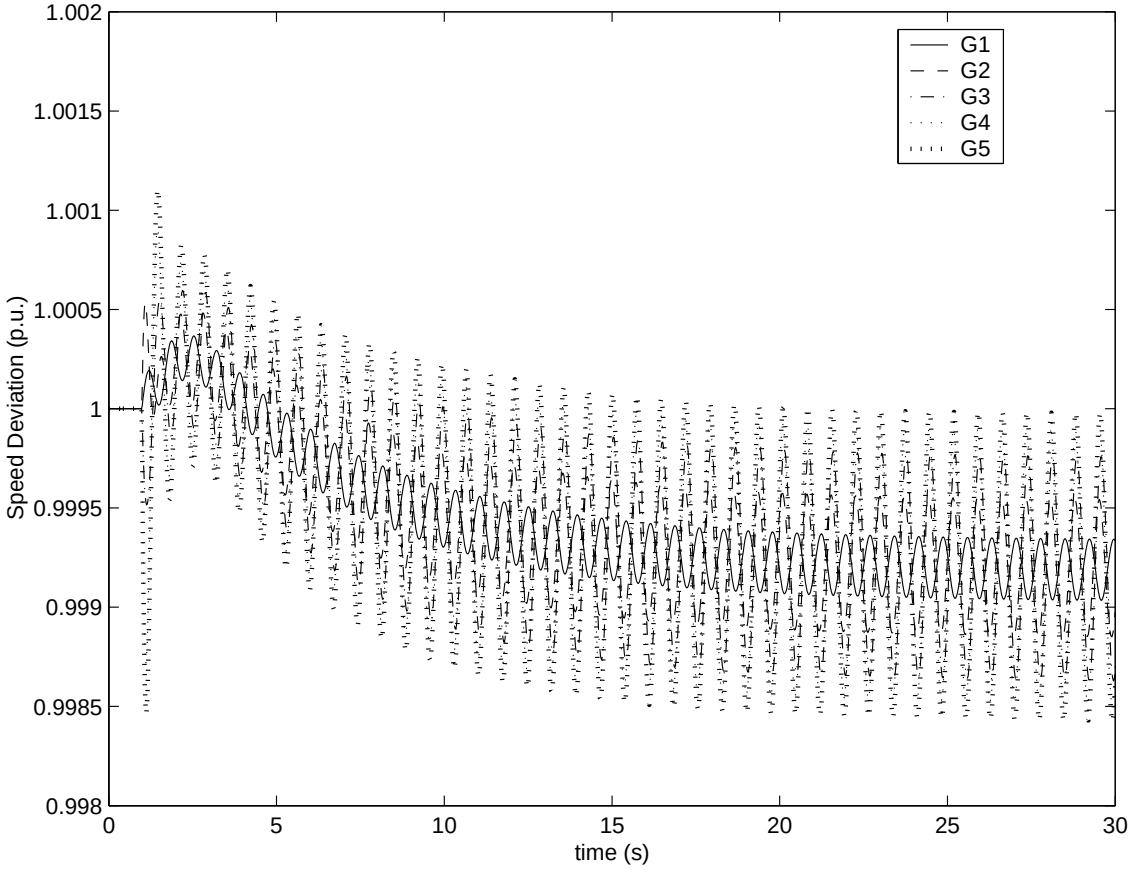

Figure 2.3: Generator speed oscillation due to Hopf bifurcation triggered by line 2-4 outage at λ=0.4 .

2.3.2 Effect of PSS Controller

The PSS controller model used in this case is shown in Figure 1.7. The gain and various time constants of the PSS were selected from [2] based on the rating of the machine. A complete set of data for the PSS controller parameters are given in Appendix B.

The best placement of the PSS controller is generator 1 [25], as it successfully removes the Hopf bifurcation in all the cases as shown in Figure 2.4. The SLM is not affected by the addition of the PSS controller, which is not the case with the addition of FACTS controllers as discussed below. Figures 2.5 and 2.6 show an eigenvalue plot and the generator speed deviation plot, respectively, for a line 2-4 outage, at the operating point $\lambda = 0.4$. These results confirm the removal of the Hopf bifurcation and the oscillation damping introduced by the PSS.

2.3.3 Effect of SVC Controller

A SVC is added to show the effect of this controller on the system. The added controller's model, which is shown in Figure 1.9, is placed on bus 14 based on loadability analysis [12]. The controller parameters are given in Appendix B for a controller rating of 200 Mvar.

Figure 2.7 shows the P-V curves of the system with the SVC. It is clear that the SLM and DLM have increased in all cases (see Table 2.2), and that the voltage profiles are also improved by the introduction of the controller, as expected.

Figure 2.8 shows some eigenvalues for the system with a SVC and the line 2-4 outage. The time domain simulation for the same condition is depicted in Figure

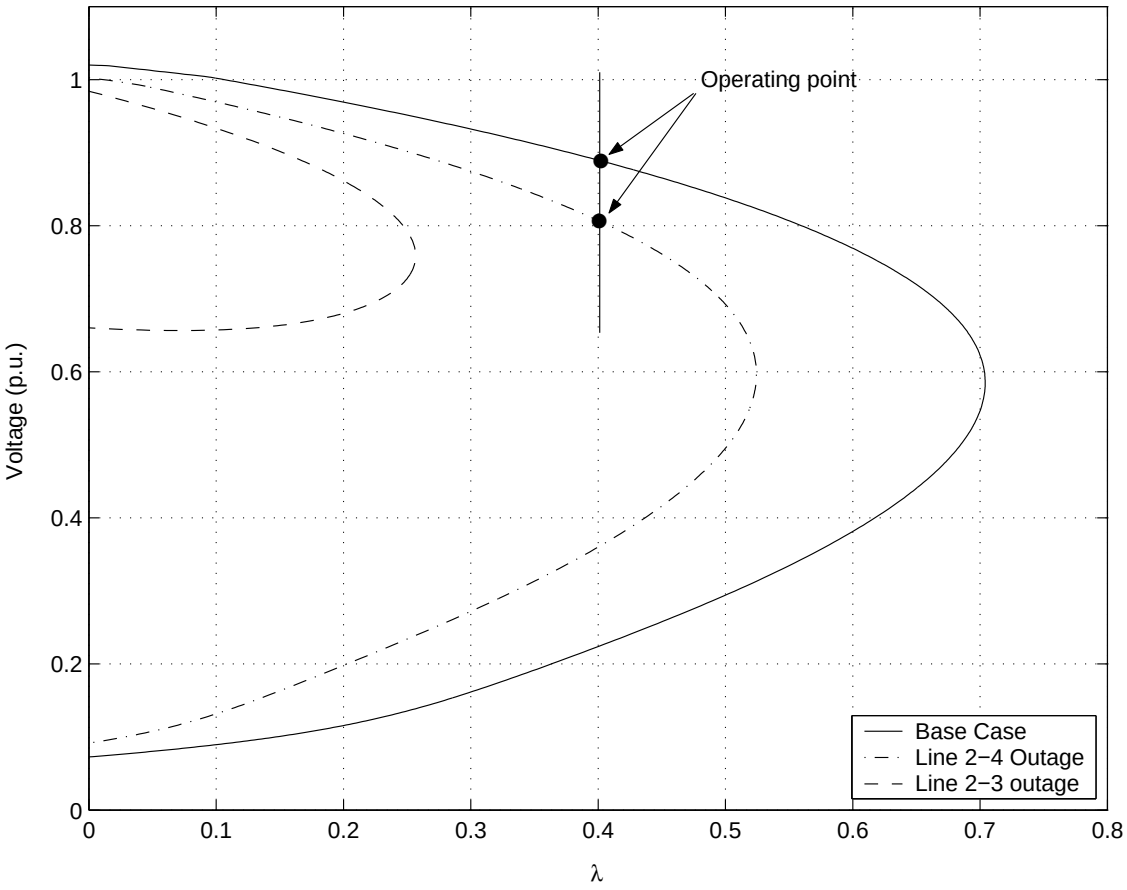

Figure 2.4: P-V curves at bus 14 for different contingencies for the IEEE 14-bus test system with a PSS at bus 1.

Table 2.2: Dynamic and Static Loading Margins for the Test System with SVC Controller

	Base Case	Line 2-4 Outage	Line 2-3 Outage
DLM (p.u.)	0.57	0.5	0.13
SLM (p.u.)	1.04	0.83	0.18

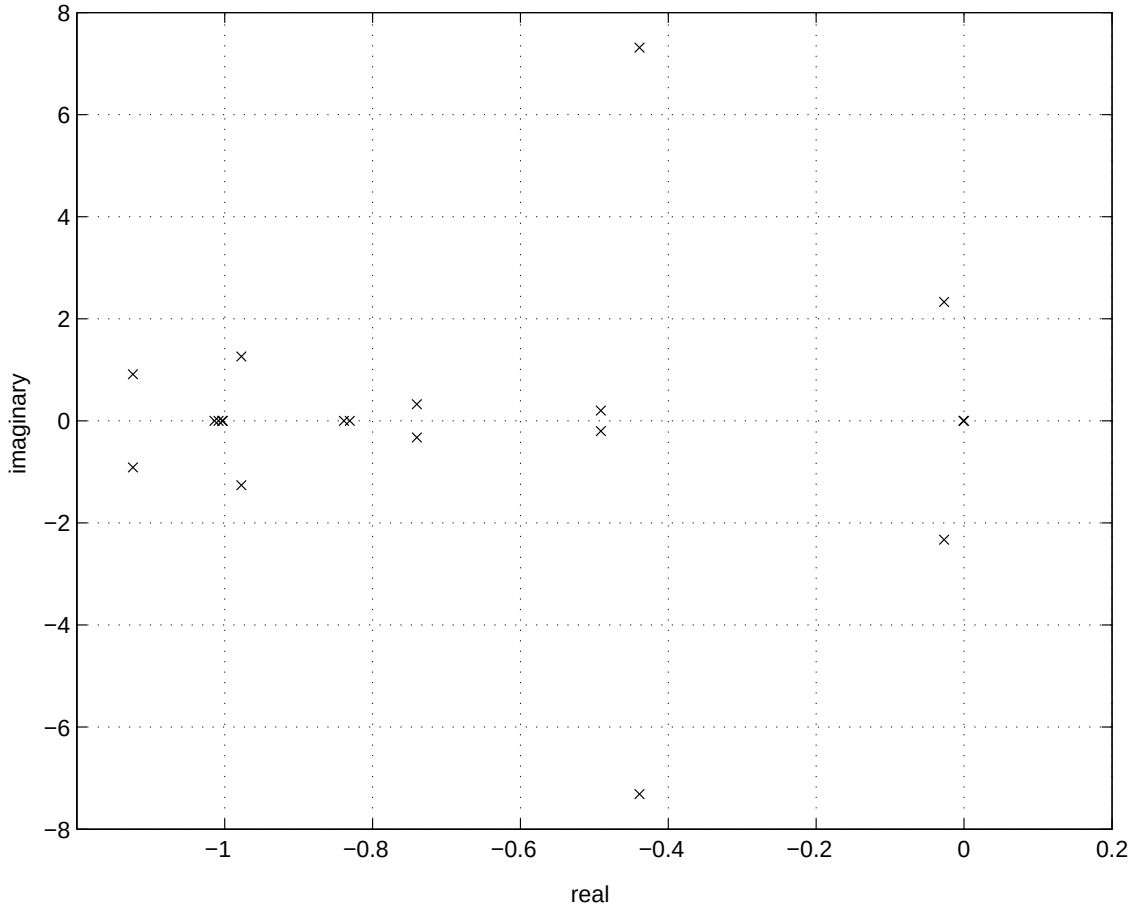

Figure 2.5: Some eigenvalues with PSS at bus 1 for a line 2-4 outage in the IEEE 14-bus test system.

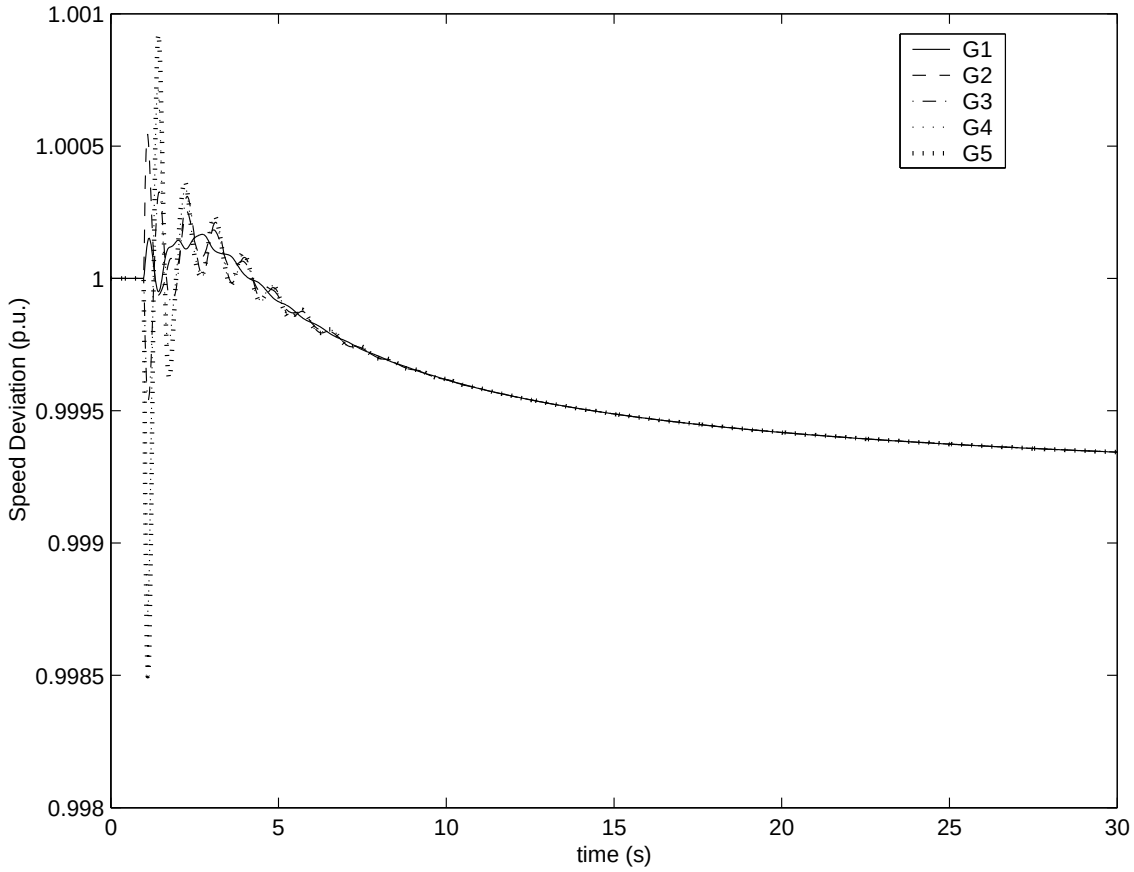

Figure 2.6: Generator speed oscillation with PSS at bus 1 for a line 2-4 outage in the IEEE 14-bus test system.

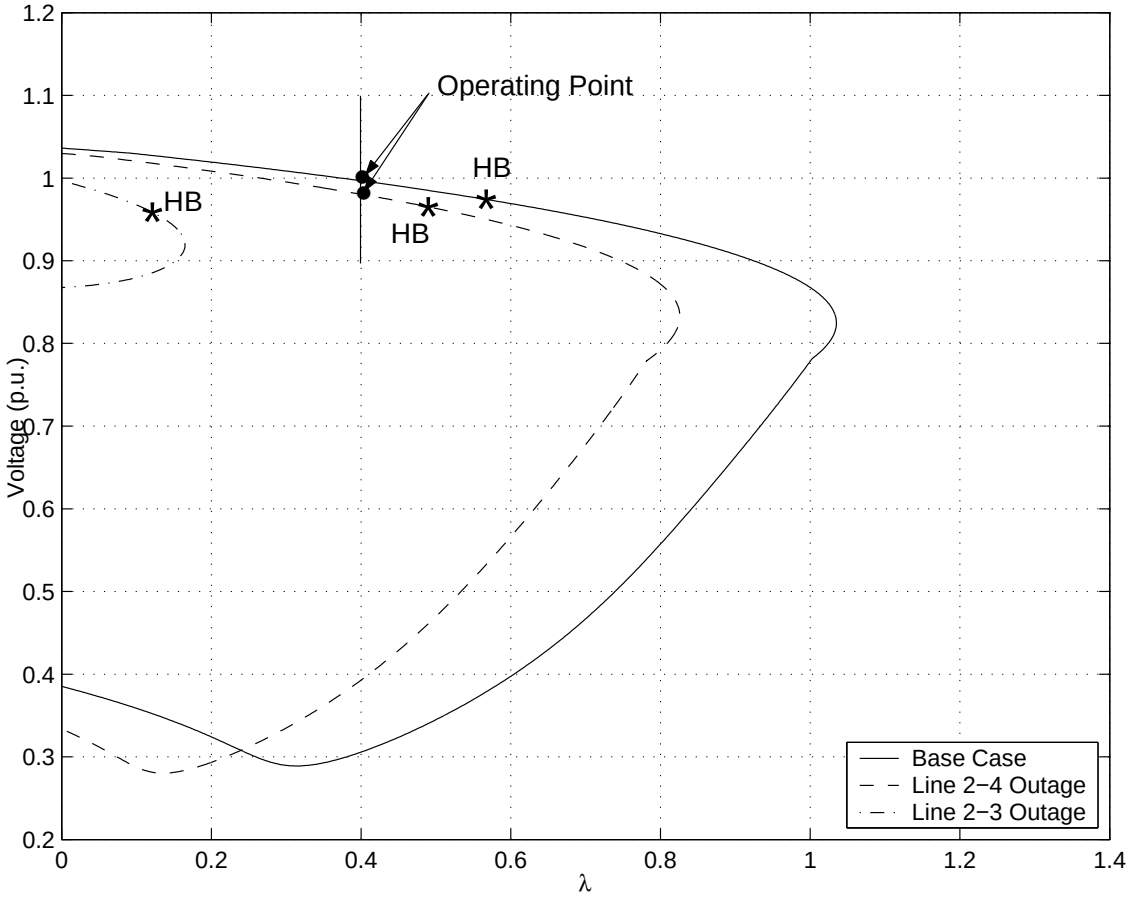

Figure 2.7: P-V curves at bus 13 for different contingencies in the IEEE 14-bus test system with a SVC at bus 14.

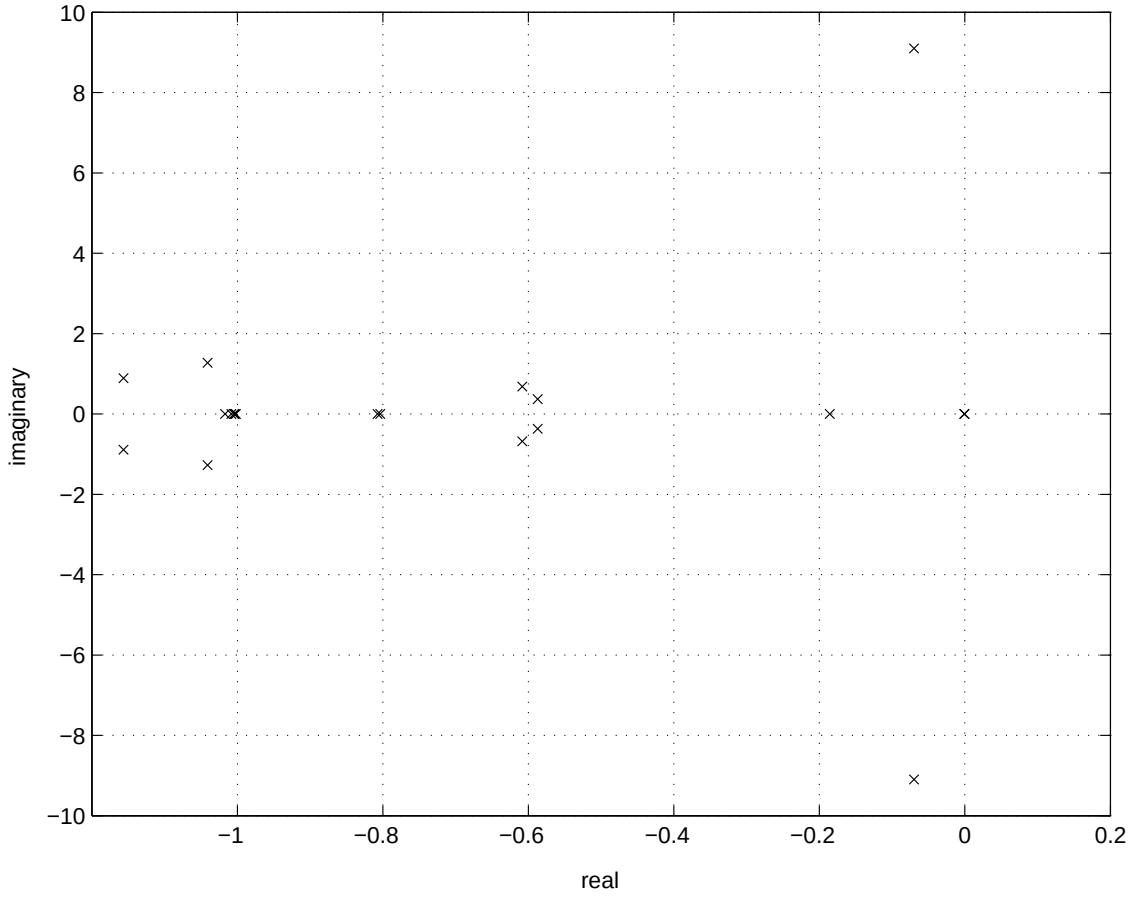

Figure 2.8: Some eigenvalues with a SVC at bus 14 for a line 2-4 outage in the IEEE 14-bus test system for $\lambda = 0.4$.

2.9. These plots demonstrate the improved system dynamic performance due to the addition of the SVC.

2.3.4 Effect of TCSC Controller

The TCSC controller is considered as another possible alternative to enhance system stability. The controller model used is depicted in Figure 1.13. Ratings and

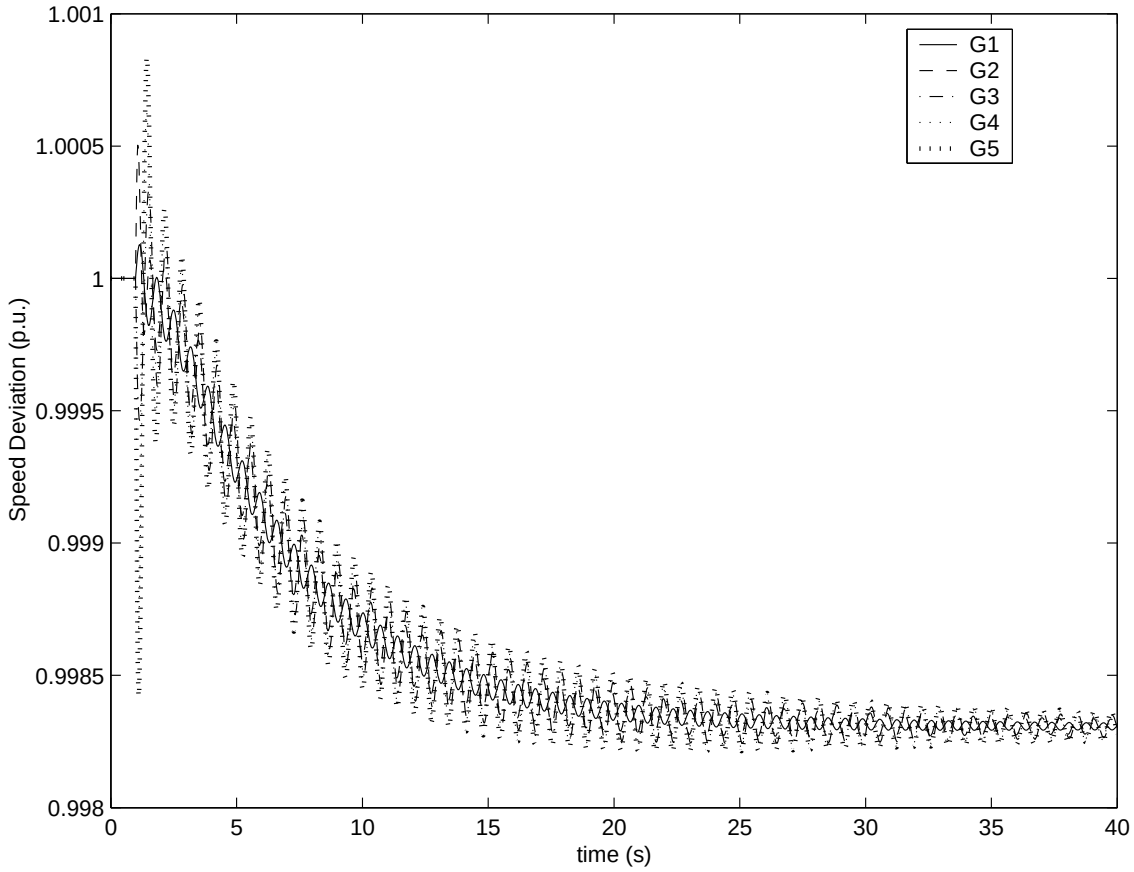

Figure 2.9: Generator speed oscillation with a SVC at bus 14 for a line 2-4 outage in the IEEE 14-bus test system for $\lambda = 0.4$.

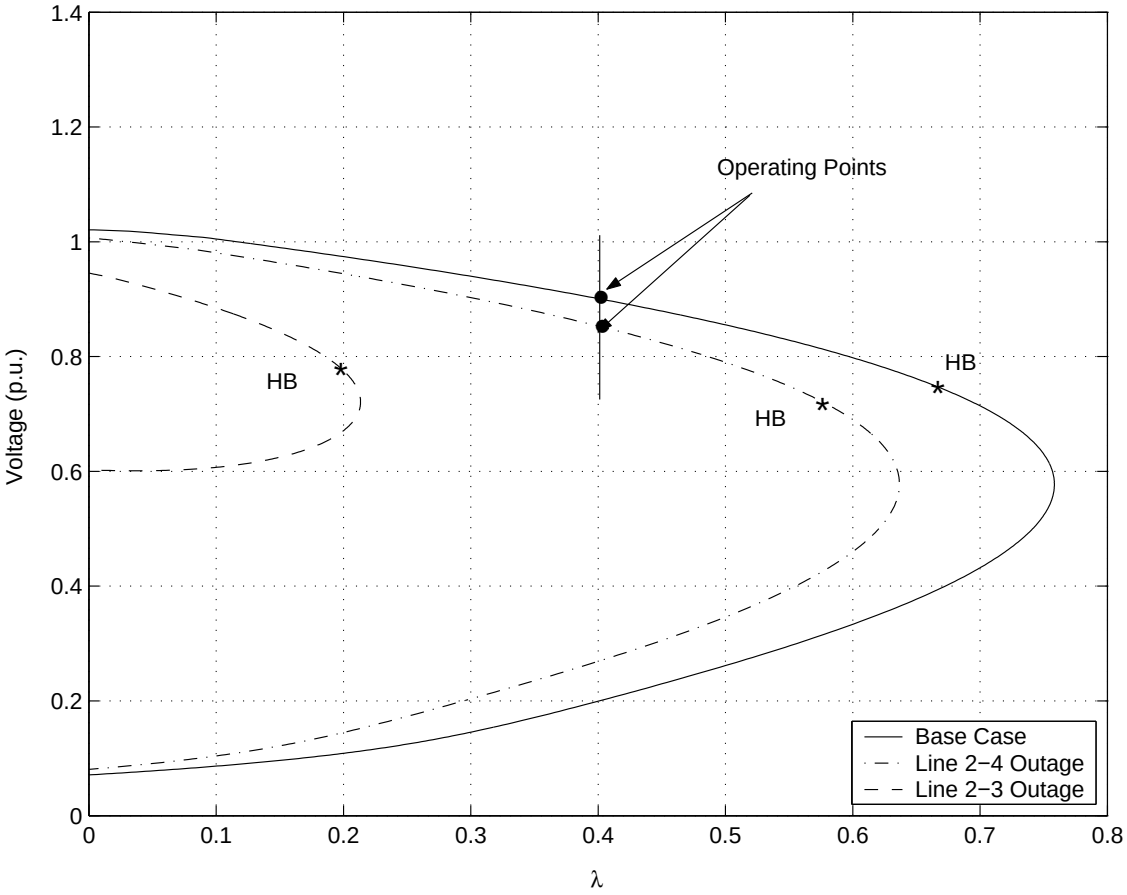

Figure 2.10: P-V curves at bus 14 for different contingencies for IEEE 14-bus test system with a TCSC in line 4-5.

controller parameters are given in Appendix B (a 40 % compensation level is assumed in this case). The placement of TCSC controller proposed in [25], i.e. in series with line 4-5, is used for the studies presented here.

Figure 2.10 shows the P-V curve for the system with the TCSC controller for the base case and two line outages. Observe that the TCSC controller positively affects the SLM and DLM of the test system, as illustrated in Table 2.3.

Figures 2.11 and 2.12 present the effect of the TCSC controller on the dynamic

Table 2.3: Dynamic and Static Loading Margins for the Test System with TCSC Controller

	Base Case	Line 2-4 Outage	Line 2-3 Outage
DLM (p.u.)	0.66	0.57	0.2
SLM (p.u.)	0.75	0.64	0.22

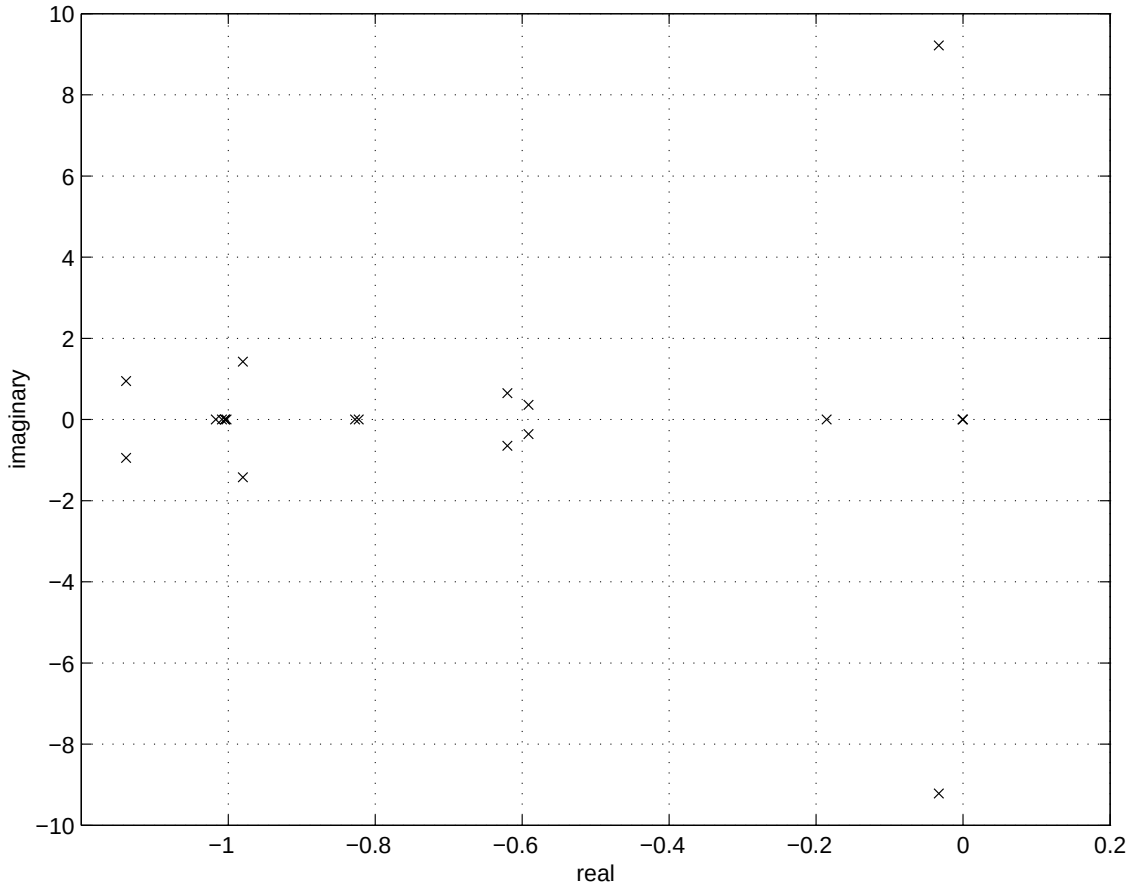

Figure 2.11: Some eigenvalues for the IEEE 14-bus test system with a TCSC in line 4-5 for line 2-4 outage.

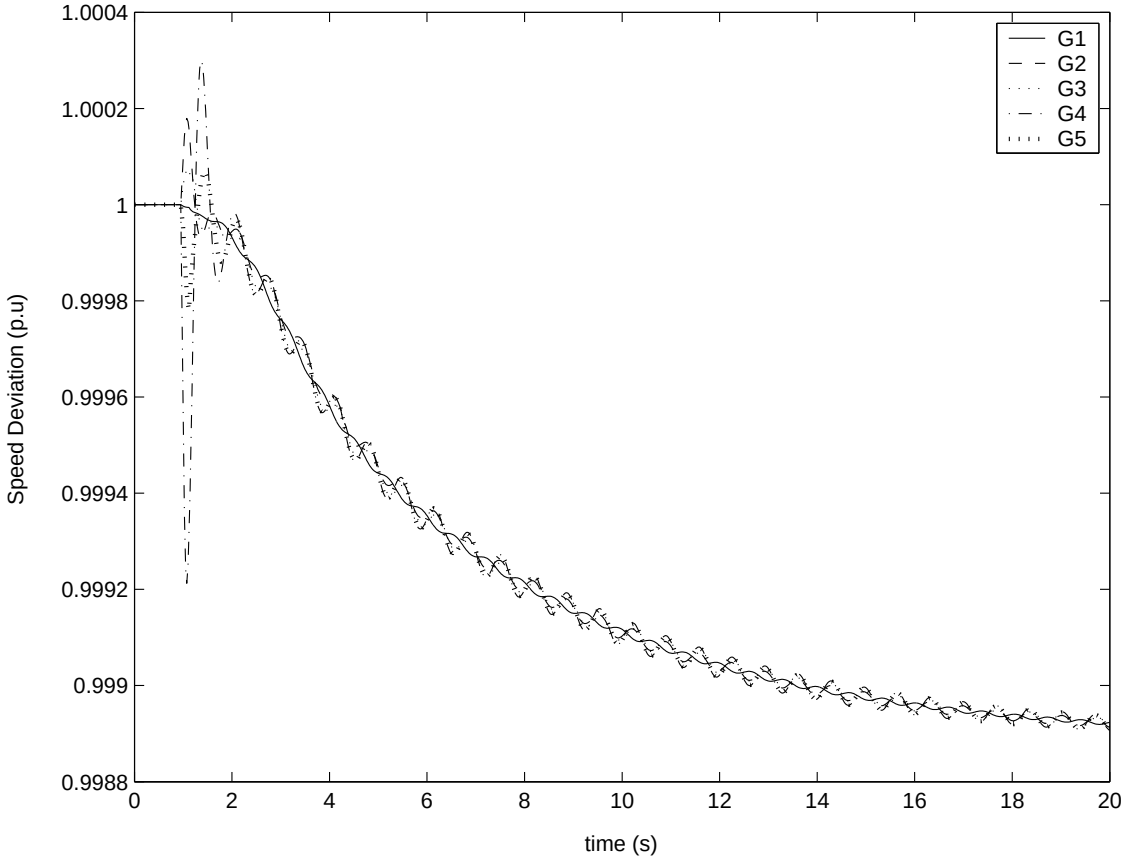

Figure 2.12: Oscillation damping in the IEEE 14-bus test system with a TCSC in line 4-5 for a line 2-4 outage.

performance of the test system. Although the system is stable, there is a lightly damped oscillations that could be improved by retuning the controller.

2.3.5 Controller Interactions Among TCSCs and PSSs

Figures 2.13 shows some eigenvalues of the system with both TCSC and PSS controllers. The value of K_{PSS} is set to 5 and the compensation ratio for the TCSC controller is 40% in this case. When K_{PSS} is increased to 7, the eigenvalues of the system are shown in Figures 2.15 and 2.14 with and without inclusion of the TCSC controller in the system. Observe the interaction between the PSS and the TCSC, which leads to an unstable operating condition, which is also confirmed by the time domain simulations shown in Figure 2.16. Hence, there is a need for retuning the PSS controller in this case to eliminate the problem generated by the addition of the TCSC controller.

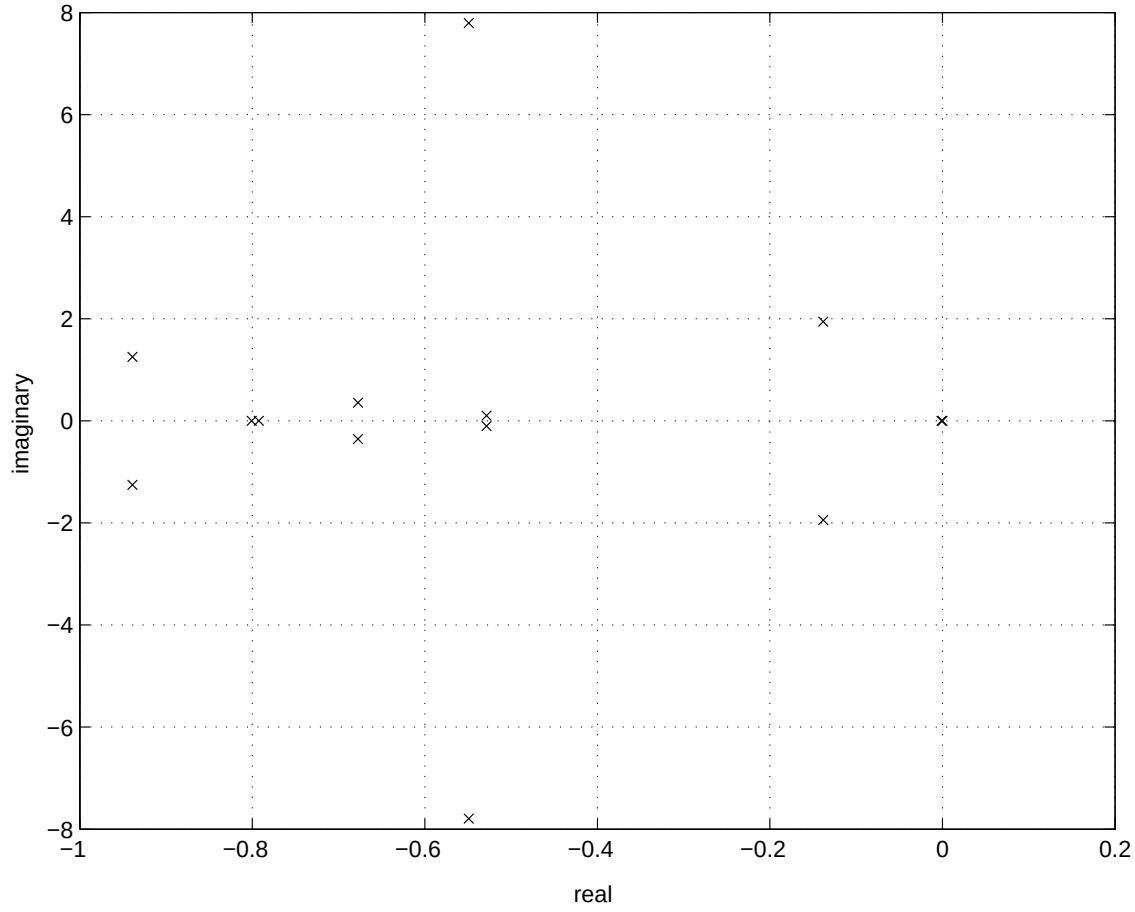

Figure 2.13: Some eigenvalues for the system with PSS controller (K_{PSS} =5) and TCSC controller for a line 2-4 outage λ =0.4.

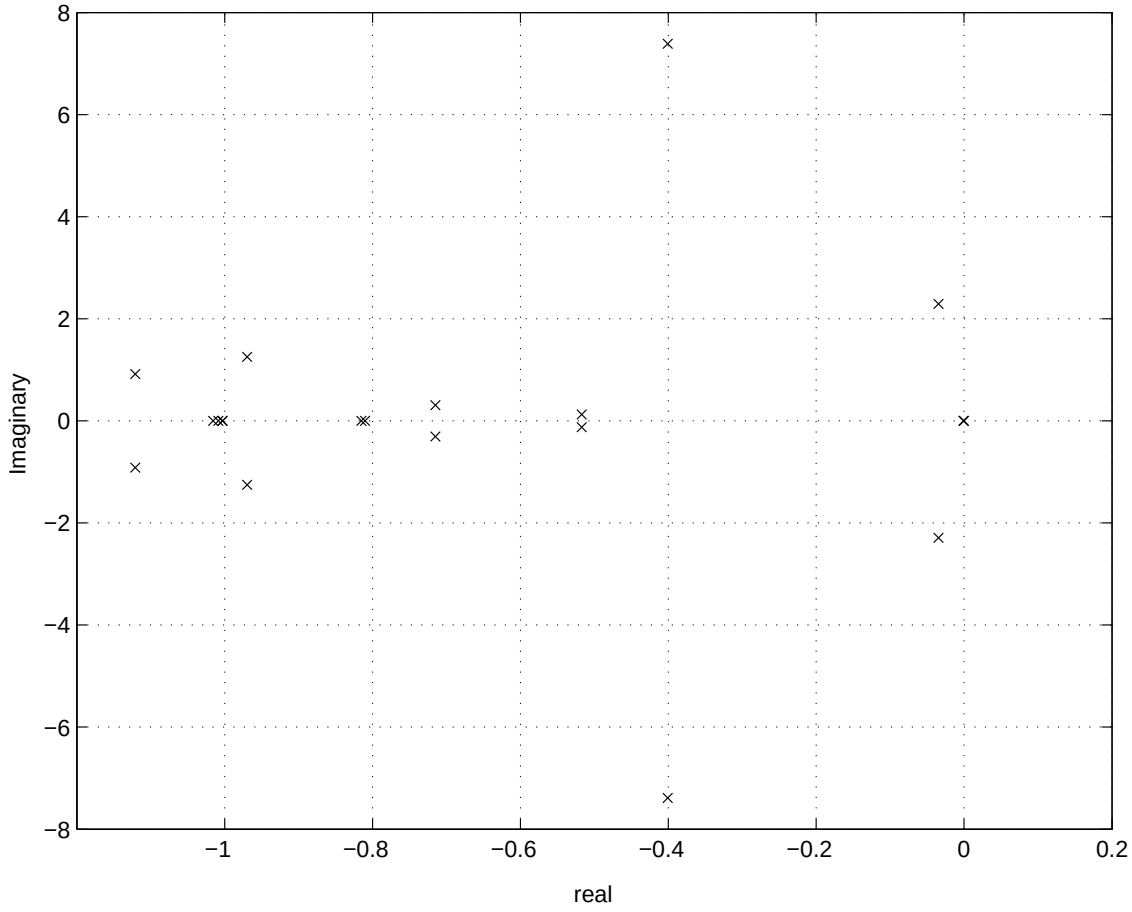

Figure 2.14: Some eigenvalues for the system with PSS controller only (K_{PSS} =7) for a line 2-4 outage at λ =0.4.

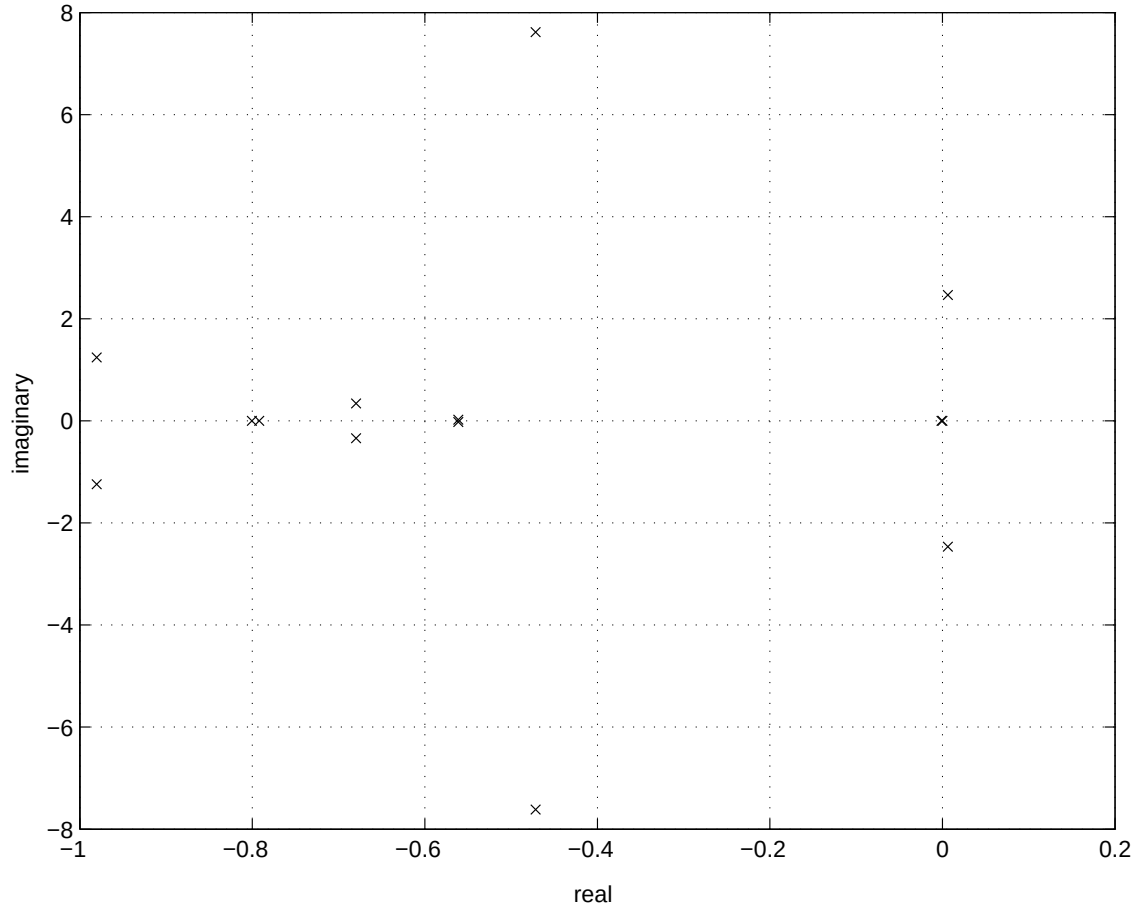

Figure 2.15: Some eigenvalues for the system with PSS controller (K_{PSS} =7) and TCSC controller for a line 2-4 outage at λ =0.4.

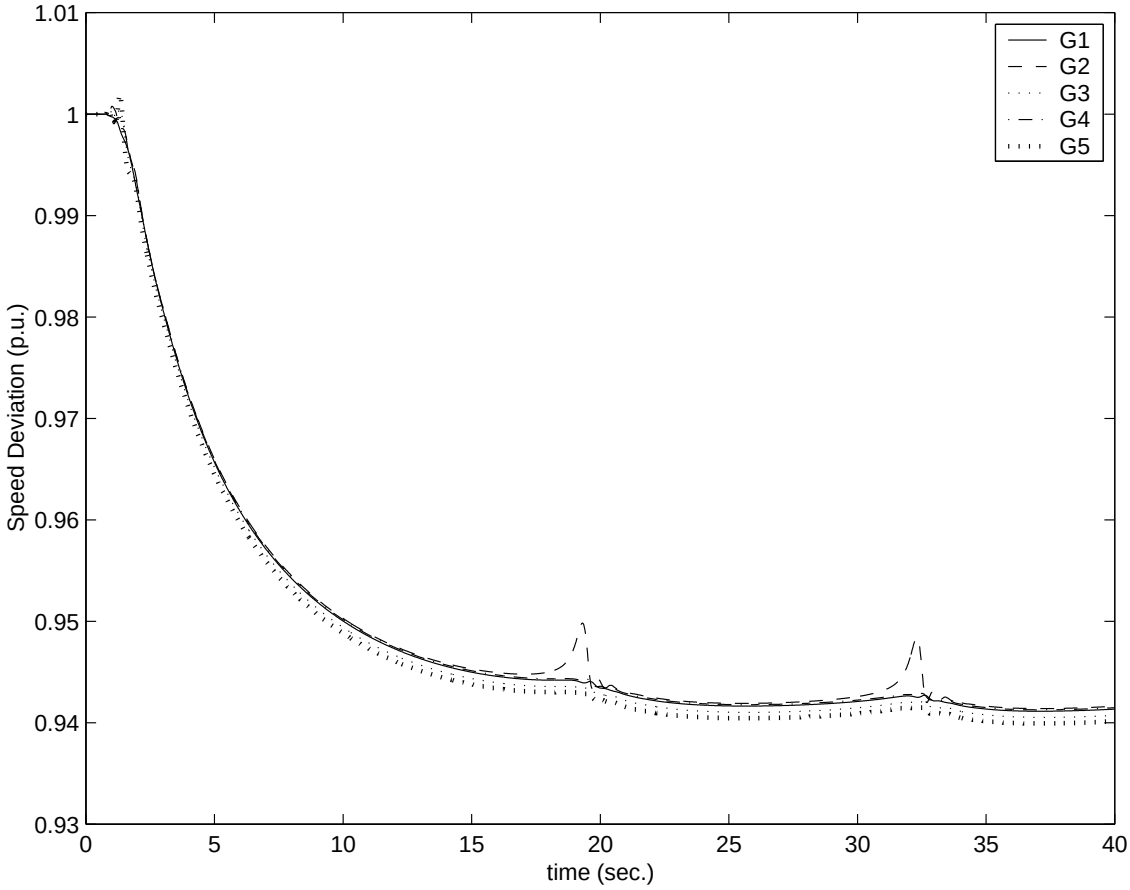

Figure 2.16: Oscillation damping in the IEEE 14-bus test system with PSS controller (K_{PSS} =7) and TCSC controller for line 2-4 outage at λ =0.4.

Appendix A

IEEE 14-BUS TEST SYSTEM

Table A.1: Exciter data

Exciter no.	1	2	3	4	5
K_A	200	20	20	20	20
T_A	0.02	0.02	0.02	0.02	0.02
T_B	0.00	0.00	0.00	0.00	0.00
T_c	0.00	0.00	0.00	0.00	0.00
V_{Rmax}	7.32	4.38	4.38	6.81	6.81
V_{Rmin}	0.00	0.00	0.00	1.395	1.395
K_E	1.00	1.00	1.00	1.00	1.00
T_E	0.19	1.98	1.98	0.70	0.70
K_F	0.0012	0.001	0.001	0.001	0.001
T_F	1.0	1.0	1.0	1.0	1.0

Table A.2: Generator data

Generator bus no.	1	2	3	4	5
MVA	615	60	60	25	25
x_l (p.u.)	0.2396	0.00	0.00	0.134	0.134
r_a (p.u.)	0.00	0.0031	0.0031	0.0014	0.0041
x_d (p.u.)	0.8979	1.05	1.05	1.25	1.25
x'_d (p.u.)	0.2995	0.1850	0.1850	0.232	0.232
x''_d (p.u.)	0.23	0.13	0.13	0.12	0.12
T'_{do}	7.4	6.1	6.1	4.75	4.75
T''_{do}	0.03	0.04	0.04	0.06	0.06
x_q (p.u.)	0.646	0.98	0.98	1.22	1.22
x'_q (p.u.)	0.646	0.36	0.36	0.715	0.715
x''_q (p.u.)	0.4	0.13	0.13	0.12	0.12
T'_{qo}	0.00	0.3	0.3	1.5	1.5
T''_{qo}	0.033	0.099	0.099	0.21	0.21
H	5.148	6.54	6.54	5.06	5.06
D	2	2	2	2	2

Table A.3: Bus data

Bus No.	P Generated (p.u.)	Q Generated (p.u.)	P Load (p.u.)	Q Load (p.u.)	Bus Type*	Q Generated max.(p.u.)	Q Generated min.(p.u.)
1	2.32	0.00	0.00	0.00	2	10.0	-10.0
2	0.4	-0.424	0.2170	0.1270	1	0.5	-0.4
3	0.00	0.00	0.9420	0.1900	2	0.4	0.00
4	0.00	0.00	0.4780	0.00	3	0.00	0.00
5	0.00	0.00	0.0760	0.0160	3	0.00	0.00
6	0.00	0.00	0.1120	0.0750	2	0.24	-0.06
7	0.00	0.00	0.00	0.00	3	0.00	0.00
8	0.00	0.00	0.00	0.00	2	0.24	-0.06
9	0.00	0.00	0.2950	0.1660	3	0.00	0.00
10	0.00	0.00	0.0900	0.0580	3	0.00	0.00
11	0.00	0.00	0.0350	0.0180	3	0.00	0.00
12	0.00	0.00	0.0610	0.0160	3	0.00	0.00
13	0.00	0.00	0.1350	0.0580	3	0.00	0.00
14	0.00	0.00	0.1490	0.0500	3	0.00	0.00

*Bus Type: (1) swing bus, (2) generator bus (PV bus), and (3) load bus (PQ bus)

Table A.4: Line Data

From Bus	To Bus	Resistance (p.u.)	Reactance (p.u)	Line charging (p.u.)	tap ratio
1	2	0.01938	0.05917	0.0528	1
1	5	0.05403	0.22304	0.0492	1
2	3	0.04699	0.19797	0.0438	1
2	4	0.05811	0.17632	0.0374	1
2	5	0.05695	0.17388	0.034	1
3	4	0.06701	0.17103	0.0346	1
4	5	0.01335	0.04211	0.0128	1
4	7	0.00	0.20912	0.00	0.978
4	9	0.00	0.55618	0.00	0.969
5	6	0.00	0.25202	0.00	0.932
6	11	0.09498	0.1989	0.00	1
6	12	0.12291	0.25581	0.00	1
6	13	0.06615	0.13027	0.00	1
7	8	0.00	0.17615	0.00	1
7	9	0.00	0.11001	0.00	1
9	10	0.03181	0.08450	0.00	1
9	14	0.12711	0.27038	0.00	1
10	11	0.08205	0.19207	0.00	1
12	13	0.22092	0.19988	0.00	1
13	14	0.17093	0.34802	0.00	1

Appendix B

DATA of the Controllers

B.1 PSS Data

Table B.1: PSS controller parameters used in the PST software

K_{pss}	T_W (s)	T_1	T_2	T_3	T_4	V_{smax}	V_{smin}
5	10	0.38	0.02	0.38	0.02	0.1	-0.1

B.2 SVC Data

Table B.2: SVC static data

X_c (p.u.)	X_l (p.u.)	α_{min} (deg.)	α_{max} (deg.)	Slope (%)	MVA	kV
1.1708	0.4925	90	175	2	200	13.8

Table B.3: SVC controller parameters used in the PST software

K	T (s)	B_{max} (p.u.)	B_{min} (p.u.)
25	0.15	2	-2

B.3 TCSC Data

Table B.4: TCSC static data

X_c (p.u.)	X_l (p.u.)	α_{min} (deg.)	α_{max} (deg.)	kV
0.00526	0.000526	155	175	69

Table B.5: TCSC controller parameters used in the PST software

T	K_w	T_w	T_1	T_2	T_3	T_4	X_{min} (p.u.)	X_{max} (p.u.)
0.015	1.1	5	1.1	0.05	0.08	0.5	0.00527	0.0514

Bibliography

[1] N. Mithulananthan, C. A. Cañizares, and J. Reeve. "Indices to Detect Hopf Bifurcation in Power Systems". In *Proc. of NAPS-2000*, pp. 15–18–15–23, October 2000.

[2] P. M. Anderson and A. A. Fouad, *Power System Control and Stability*. IEEE Press, 1994.

[3] P. Kundur, *Power System Stability and Control*. McGraw Hill, New York, 1994.

[4] J. Arrillaga and C. P. Arnold, *Computer Analysis of Power Systems*. John Wiley & Sons, England, 1990.

[5] R.P. schulz. "Synchronous Machine Modeling. Symposium on Adequency and Philosophy of Modeling System Dynamic Performance". In *IEEE Pub. 75 CH O970-PWR*, 1975.

[6] P. M. Anderson and A. A. Fouad, *Power System Control and Stability*. The Iowa State University Press, AMES, IOWA, U.S.A., 1977.

[7] N. Mithulananthan, M. M. A. Salama, C. A. Cañizares, and J. Reeve, "Distribution System Voltage Regulation and Var Compensation for Different Static Load Models," *IJEEE*, vol. 37, no. 4, October 2000, pp. 384–395.

[8] IEEE FACTS working group 15.05.15, "FACTS Application", December 1995.

[9] N. Yang, Q. Liu, and J. D. McCalley, "TCSC Controller Design for Damping Interarea Oscillations," *IEEE Trans. on Power Systems*, vol. 13, no. 4, November 1998, pp. 1304–1309.

[10] M. J. Lautenberg, M. A. Pai, and K. R. Padiyar, "Hopf Bifurcation Control in Power System with Static Var Compensators," *Int. J. Electric Power and Energy Systems*, vol. 19, no. 5, 1997, pp. 339–347.

[11] N. G. Hingorani, "Flexible AC Transmission Systems," *IEEE Spectrum*, April 1993, pp. 40–45.

[12] C. A. Cañizares and Z. T. Faur, "Analysis of SVC and TCSC Controllers in Voltage Collapse," *IEEE Trans. on Power Systems*, vol. 14, no. 1, February 1999, pp. 158–165.

[13] L. Gyugyi, "Dynamic Compensation of AC Transmission Lines by Solid State Synchronous Voltage Sources," *IEEE Trans. on Power Systems*, vol. 9, no. 2, April 1994, pp. 904–911.

[14] L. Gyugyi, N. G. Hingorani, P. R. Nannery, and N. Tai, *" Advanced Static Var Compensators using Gate Turn-off Thyristors for Utility Application"*. CIGRE 23-203, August 1990.

[15] E. Uzunovic, C. A. Cañizares, and J. Reeve. "Fundamental Frequency Model of Static Synchronous Compensator". In *Proc. North American Power Symposium*, pp. 49–54, Laramie, Wyoming, October 1997.

[16] C. A. Cañizares. "Power Flow and Transient Stability Models of FACTS Con-

trollers for Voltage and Angle Stability Studies". In *Proc. of IEEE/PES Winter Meeting*, Singapore, January 2000.

[17] G. Hingorani and L. Gyugi, *Understanding FACTS: Concepts and Technology of Flexible AC Transmission Systems*. IEEE Press, 1999.

[18] N. Martins, H. Pinto, and J. Paserba. "Using a TCSC for Power System Scheduling and System Oscillation Damping-Small Signal and Transient StabilityStudies". In *Proc. IEEE/PES Winter Meeting*, Singapore, January.

[19] *Impact of Interactions Among System Controllers*. CIGRE Task Force 38.02.16, November 1999.

[20] A. D. Del Rosso, C. A. Cañizares, and V. M. Doña, "A Study of TCSC Controller Design for Power System Stability Improvement," *Accepted to IEEE Trans. on Power Systems*, September 2002.

[21] J. Paserba, N. Miller amd E. larsen, and R. Piwko, "A Thyristor Series Controlled Compensation Model for Power System Stability Analysis ," *IEEE Trans. on Power Systems*, vol. 10, no. 4, November 1995, pp. 1471–1478.

[22] C. A. Cañizares, *UWPFLOW: Continuation and Direct Methods to Locate Fold Bifurcation in AC/DC/FACTS Power Systems*. University of Waterloo, November 1999. Available at http://www.power.uwaterloo.ca.

[23] *Power System Toolbox Version 2.0: Load Flow Tutorial and Functions*. Cherry Tree Scientific Software, RR-5 Colborne, Ontario K0K 1S0, 1991-1999.

[24] *Power System Toolbox Version 2.0: Dynamic Tutorial and Functions*. Cherry Tree Scientific Software, RR-5 Colborne, Ontario K0K 1S0, 1991-1997.

[25] N. Mithulananthan. *Hopf Bifurcation Control and Indices for Power System with Interacting Generator and FACTS Controllers.* PhD thesis, University of Waterloo, Waterloo, ON, Canada, 2002. Available at http://www.uwaterloo.ca.